

A Matrix Product State Model for Simultaneous Classification and Generation

Alex Mossi*, Bojan Žunkovič†, Kyriakos Flouris‡

**D-MATH, ETH Zürich, amossi@ethz.ch*

†*FRI, University of Ljubljana, bojan.zunkovic@uni-lj.si*

‡*D-ITET, ETH Zürich, kflouris@ethz.ch*

Abstract—Quantum machine learning (QML) is a rapidly expanding field that merges the principles of quantum computing with the techniques of machine learning. One of the powerful mathematical frameworks in this domain is tensor networks. These networks are used to approximate high-order tensors by contracting tensors with lower ranks. Originally developed for simulating quantum systems, tensor networks have become integral to quantum computing and, by extension, to QML. Their ability to efficiently represent and manipulate complex, high-dimensional data makes them suitable for various machine learning tasks within the quantum realm. Here, we present a matrix product state (MPS) model, where the MPS functions as both a classifier and a generator. The dual functionality of this novel MPS model permits a strategy that enhances the traditional training of supervised MPS models. This framework is inspired by generative adversarial networks and is geared towards generating more realistic samples by reducing outliers. Additionally, our contributions offer insights into the mechanics of tensor network methods for generation tasks. Specifically, we discuss alternative embedding functions and a new sampling method from non-normalized MPSs.

I. INTRODUCTION

In recent years, quantum technologies have undergone rapid and substantial advancements, holding the promise of revolutionizing various scientific and industrial domains [1]. These advancements are closely intertwined with quantum machine learning (QML) [2], [3], and tensor networks (TNs) emerging as a vital mathematical tool. Central to the concept of TNs is their ability to approximate high-dimensional tensors via memory-efficient multidimensional arrays [4]. Originally devised as tools for the approximation and simulation of quantum systems within the domains of many-body quantum physics [5] and condensed matter physics [6], TNs now encompass a diverse array of fields, including data compression [7], privacy [8], and high-dimensional PDEs [9]. Of particular interest is their application in machine learning for both supervised [10] and unsupervised tasks [11]–[13].

Prominent tensor networks in contemporary research include Projected Entangled Pair States (PEPS) [13], Matrix Product State (MPS) [10] [11], Locally Purified State (LPS) [14], Multiscale Entanglement Renormalization Ansatz (MERA) [15], Tree Tensor Networks (TTN) [16] and isometric tensor networks [17]. Of note, MPS, characterized by rank-3 tensors and sequential 1-dimensional contractions, has garnered considerable attention due to its relative simplicity and versatility [18].

MPSs were originally used to describe and simulate the quantum states of one-dimensional systems since they can faithfully represent quantum states featuring limited entanglement [19] [20] [21]. Such systems are notoriously challenging owing to the curse of dimensionality, which arises from the exponential growth of Hilbert spaces in such contexts [22]. Since then, MPSs have been adapted to address a wide spectrum of datasets, including two-dimensional systems [23], rendering them suitable for image processing in machine learning applications. This has led to their successful application in tasks such as image classification using datasets like MNIST [24] and Fashion MNIST [25]. While early training methods for MPSs in machine learning relied on Density Matrix Renormalization Group (DMRG) techniques [10], contemporary machine learning libraries provide more accessible approaches [26] based on automatic differentiation [27], [28].

MPS models are typically employed for conventional classification [10] or as generators in unsupervised contexts [11]. However, the distinctive structure of MPS, combined with the characteristics of the embedding functions employed in this work, allows the use of a single model for both classification and generation tasks [29]. This enables the use of a GAN-style method to improve its generative performance without affecting its classification accuracy.

We propose a novel approach for training supervised MPSs in a GAN-style setting, as detailed in Sec. II-C. The MPS serves as both a classifier and a generator, resulting in improved generative performance and a reduction in the number of outliers generated. To this end, we present several contributions that allow the realization of such a model while providing insights into the mechanics of tensor-network methods for generation tasks. First, we provide a brief introduction to Matrix Product States, demonstrating their canonical forms and explaining why these forms are not strictly required in a machine learning setting.

Second, we discuss the essential characteristics of the embedding functions employed to transform input data into a format compatible with MPS structures. Third, we present alternative embedding functions that facilitate the computation of the marginalized probability density function (PDF) over a single variable, $p(x_i)$, without requiring the evaluation of multidimensional integrals. Fourth, we introduce an exact sampling procedure from non-normalized MPS.

The second part of this work, Sec. II-B focuses on machine learning applications of MPS. We propose implementing MPS

$$W = \sum_{\{\alpha\}} A_1^{\alpha_1} A_2^{\alpha_1 \alpha_2} \dots A_N^{\alpha_{N-1}} = \quad (5)$$

$$= \sum_{\{\alpha\}} A_1^{\alpha_1} X_1 X_1^{-1} A_2^{\alpha_1 \alpha_2} X_2 \dots X_{n-1}^{-1} A_N^{\alpha_{N-1}} = \quad (6)$$

$$= \sum_{\{\alpha\}} B_1^{\alpha_1} B_2^{\alpha_1 \alpha_2} \dots B_j^{\alpha_j \alpha_{j+1}} \dots B_N^{\alpha_{N-1}}, \quad (7)$$

proving the non-uniqueness of the representation of an MPS. These degrees of freedom are termed 'gauge' degrees of freedom. The non-unique representation of MPSs is exploitable and can help devise better privacy-preserving machine learning algorithms [34]. Canonical forms are also crucial for an efficient time-dependent variational principle for MPS. [35].

To establish a canonical form for the MPS, various methods can be employed. One method uses DMRG-based and singular value decomposition techniques [31]. Another alternative [36] employs the QR decomposition of the matrices that compose the MPS to achieve an orthogonal decomposition of the matrices. Those canonical forms of MPSs are needed to describe a so-called sweeping algorithm used for optimization [37]. However, canonical forms can often be difficult to obtain for arbitrary MPSs [38], since some of the calculation needed (for example, calculating the optimal rank d) are NP-hard [39] and/or a ill-posed problem [40]. The sweeping algorithm and its necessary calculation of a canonical form will not be required as we can effectively leverage a more accessible approach via PyTorch automatic differentiation [41], discussed in Sec. II-B1. We use an approach often used for tensor networks applied in machine learning scenarios [26].

2) *Embedding function*: If the objective is data classification, the embedding function should primarily introduce non-linearity and transform the data such that our MPS can effectively achieve linear separation in the high-dimensional space where the data is embedded. Conversely, if the model is being used for data sampling, there is a greater emphasis on the selection of the embedding function. To employ the methodology outlined in Sec. II-B2 and perform simultaneous classification and generation tasks, an essential prerequisite for the embedding function $\Phi(x) = \bigotimes_{i=1}^d \phi(x_i)$ is as follows:

$$\int_{x \in X} \phi_i(x) \phi_j(x), dx = \delta_{i,j}, \quad (8)$$

where $X = [0, 1]$, assumed to be the support of the input data, with limited exceptions noted herein. Eq. 8 allows for a greatly simplified computation of the marginal probability over single variables, avoiding high-dimensional integrals as shown in Sec. II-A3. In certain cases, the embedding functions may also be defined with

$$\int_{x \in X} \phi_i(x) \phi_j(x) = c \cdot \delta_{i,j}, \quad c > 0. \quad (9)$$

Such a condition yields a non-normalized PDF. Nevertheless, we demonstrate that our method can accommodate any resulting inconsistencies, Sec. II-B2, II-B3.

The marginal probability over a single variable will have the form of

$$P(x_i) = \phi(x_i) \cdot V_i \cdot \phi(x_i), \quad (10)$$

with V_i being the symmetric and semi-positive definite reduced density matrix, Sec. II-A3. This implies that the PDF and its complexity will depend on our choice of $\phi(x)$ and the physical dimension of the model.

In the case of handling simple low-frequency data, such as high-contrast or binary images, a common embedding function [12] [10] is given by:

$$\phi(x) = [\sin(\frac{\pi}{2}x), \cos(\frac{\pi}{2}x)]. \quad (11)$$

This adheres to the constraint specified in Eq. 8 over the interval $[-1, 1]$. However, this function exhibits a limitation in that it possesses a low physical dimension of only 2. Consequently, for certain datasets, it may struggle to introduce the requisite complexity, thereby potentially impeding the model's performance.

A generalized replacement, outlined in [10], involves the use of the embedding function:

$$\phi_i(x) = \sqrt{\binom{d-1}{i-1}} \cos(x)^{d-i} \sin(x)^i. \quad (12)$$

This function belongs to the class of functions referred to as spin coherent states [10]. However, Eq. 12 does not satisfy the condition specified in Eq. 8 and is therefore not a candidate embedding function for generation.

An alternative proposal is the Fourier embedding [42]:

$$\phi_i(x) = \cos(i\pi x), \text{ for } i \in \{0, \dots, d-1\}, \quad (13)$$

for $\text{Supp}(\Phi) = [0, 1]^n$. This feature map satisfies Eq. 8 and can model more general PDFs, due to the fact that we can use arbitrarily high values of d . In this case, the PDF over a single variable will be modeled by the following equation:

$$\sum_{i=0}^{d-1} \sum_{j=0}^{d-1} a_{ij} \cos(\frac{\pi}{2}ix) \cos(\frac{\pi}{2}jx). \quad (14)$$

Our alternative proposal for an embedding function for high-dimensional physical spaces is to leverage polynomials, and due to Eq. 8, a natural choice is the use of Legendre polynomials. These are a set of polynomials $\{P_1(x), P_2(x), \dots\}$ such that $P_i(x)$ is a polynomial of degree i and any 2 polynomials satisfy Eq. 8, obtained recursively by

$$P_0(x) = 1, \quad (15)$$

$$P_1(x) = x, \quad (16)$$

$$P_i(x) = \frac{(2i-1)xP_{i-1} - (i-1)P_{i-2}(x)}{i}, \quad \forall i \geq 2. \quad (17)$$

Unlike Fourier embeddings, $\text{Supp}(P) = [-1, 1]^N$ instead of the previous interval $[0, 1]^N$, so P will require rescaling in a pre-processing step. This embedding leads to a PDF over a single variable which is modelled by a non-negative polynomial of degree d^2 over $[-1, 1]$.

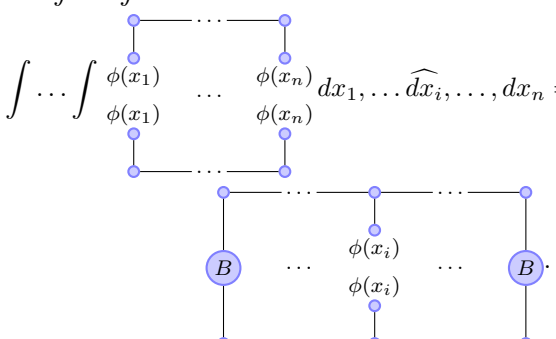
Fourier and Legendre embeddings can be used with arbitrarily large physical dimensions, thus suitable for modelling

multi-modal probability distribution functions during the generative phase of Sec. II-B2. The generative results of these embedding functions are discussed in Sec. III.

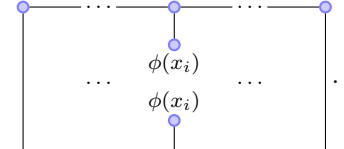
3) *Computing the reduced density matrix*: Given any embedding function $\phi(x)$, we define the following matrix:

$$B := \int \frac{\phi(x)}{\phi(x)} dx. \quad (18)$$

This is in contrast to [43], where the reduced density matrix is described by unitary tensor networks. Recalling that the PDF is approximated by an MPS by Eq. 2, the marginalized PDF can be simplified over a single variable $p(x_i)$ without necessitating the evaluation of multi-dimensional integrals:

$$\begin{aligned} p(x_i) &= \int \dots \int p(x_1, \dots, x_n) dx_1 \dots \widehat{dx}_i, \dots dx_n = \\ &= \int \dots \int \frac{\phi(x_1)}{\phi(x_1)} \dots \frac{\phi(x_n)}{\phi(x_n)} dx_1, \dots \widehat{dx}_i, \dots, dx_n = \\ &= \int \dots \int \frac{\phi(x_1)}{\phi(x_1)} \dots \frac{\phi(x_n)}{\phi(x_n)} dx_1, \dots \widehat{dx}_i, \dots, dx_n = \end{aligned} \quad (19)$$


We assume that the selection of $\phi(x)$ satisfies Eq. 8 such that $B = \mathbb{I}_d$, leading to

$$p(x_i) = \int \dots \int \frac{\phi(x_1)}{\phi(x_1)} \dots \frac{\phi(x_n)}{\phi(x_n)} dx_1, \dots \widehat{dx}_i, \dots, dx_n. \quad (20)$$


The marginalized distribution over a single variable is given by Eq. 10.

In the case where we want to calculate a conditional probability given some other variables' value, we can substitute the value of the conditioning variables. This conditional probability density over a single variable is given by:

$$p(x_i | \{x_j\}_{j \in \mathcal{I}}) = \phi(x_i) \cdot V_{i, \{x_j\}_{j \in \mathcal{I}}} \cdot \phi(x_i). \quad (21)$$

In order to compute the density matrix $V_{i, \{x_j\}_{j \in \mathcal{I}}}$, for $\{x_j | j \in \mathcal{I}\}$, we perform a contraction operation involving two copies of the MPS. At each site, there are three possible scenarios for the tensor contraction in the physical dimension:

- 1) For $j = i$, we leave these two indices open.
- 2) For $j \in \mathcal{I}$, we compute the embedding $\phi(x_j)$ and contract the physical indices at site j of the two copies of the MPS with $\phi(x_j)$.
- 3) For $j \notin \mathcal{I}$, we directly contract the open indices of the two copies of the MPS, as described visually in Eq. 20.

The outcome of this function is a semi-positive definite symmetric matrix, a real matrix M is semi-positive definite if and only if there exists a matrix B such that $M = B^\top B$. Without loss of generality and supposing $\mathcal{I} = \{1, \dots, i-1\}$, B is defined as

$$B_i := \begin{array}{c} \textcircled{A_1} \cdots \textcircled{A_{i-1}} \textcircled{A_i} \textcircled{A_{i+1}} \cdots \textcircled{A_n} \\ \downarrow \quad \quad \quad \downarrow \quad \quad \quad \downarrow \quad \quad \quad \downarrow \\ \phi(x_1) \quad \quad \quad \phi(x_{i-1}) \end{array}. \quad (22)$$

After reformatting $B_i^{d_1, d_2, \dots, d_n}$ into matrix form B'_i of shape $d^{n-i-1} \times d$, where we let the first index of the matrix correspond to the physical index of A_i and we regroup the remaining physical indices of $\{A_{i+1}, \dots, A_n\}$ as the second index of the matrix, the tensor contraction $\sum_{j_{i+1}, \dots, j_n} B_{j_1, \dots, j_{i-1}, B_{j_1, \dots, j_{i-1}}}$ will correspond to the matrix multiplication $B'_i{}^\top B'_i$. We can rewrite $V_i = B'_i B'_i{}^\top$, proving its semi-positive definiteness.

Throughout this section, we did not assume to have a normalized MPS since that will not be the case during the training procedure. This can cause the computed PDFs to be unnormalized, but this will not affect our methods of classification and sampling, as we will see later in Sec. II-B2.

B. Classification and generation

1) *Classification with MPS*: In this section, we will discuss two methods that are commonly employed to perform classification using MPSs [10]. The first approach involves creating an ensemble of MPSSs, where each MPS corresponds to a distinct label class within the data. This ensemble model generates an output vector of length C , where each component of the vector arises from the contraction of a different MPS with the input. In Fig. 2 we show these contraction steps for a single component of the ensemble.

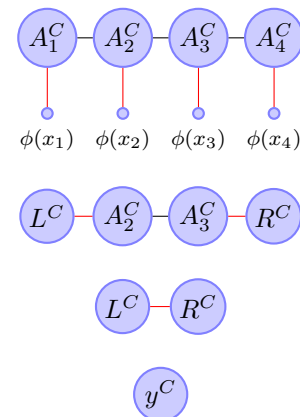


Fig. 2: This figure illustrates an example of how a single MPS of the ensemble, corresponding to the class C , and input are contracted in the forward pass, considering the case $N = 4$. The red lines indicate the indices that are being contracted in each step. By squaring the value of the final scalar y^C , we get a non-normalized probability, i.e. $p(c = i | x) = \frac{1}{Z} \cdot y_i^2$, with $Z = \sum_c y_c^2$ being a normalization constant depending on the outputs of the ensemble of MPSSs.

The second approach utilizes a single modified MPS, where we introduce an additional tensor placed in the middle of the tensor network. This supplementary tensor, with dimensions (C, D, D) , plays a crucial role in producing the desired vector of length C . The network structure of this approach is described by the following equation:

$$W_c^{d_1, d_2, \dots, d_n} = \sum_{\alpha} A_1^{\alpha_1 d_1} A_2^{\alpha_1 \alpha_2 d_2} \dots C_c^{\alpha_n / 2 \alpha_n / 2 + 1} \dots A_N^{\alpha_{N-1} d_N}, \quad (23)$$

and is also illustrated graphically in Fig. 3. The contraction of the model during the forward pass with this additional tensor are similar to the ones of the single MPS, and can be visualized in Fig. 4.

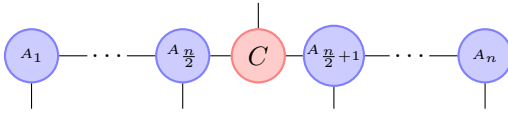


Fig. 3: The figure illustrates the MPS architecture used for classification in the case of an additional central tensor. The blue tensors constitute the MPS, while the red component represents the additional tensor that enables multiple label classes for classification.

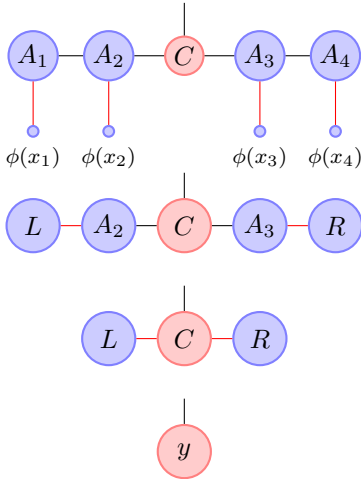


Fig. 4: This figure illustrates an example of how MPS and inputs are contracted in the forward pass of the classification, considering the case $N = 4$. The red lines indicate the indices that are being contracted in each step.

An ensemble of MPSs is fundamentally equivalent to the single MPS with the additional central tensors. Each matrix in the single MPS must be block-diagonal with bond dimension $d * C$ and blocks of size d , where each of those blocks corresponds to a different MPS from the ensemble. The primary advantage of using a single model with an additional tensor is the capability to store and compute everything with just one MPS. This contrasts with the ensemble approach, which requires multiple MPSs. For instance, the MPS with a central tensor can be effective for low-dimensional inputs with

a low bond dimension. However, in cases involving higher-dimensional data with a higher bond dimension, using an ensemble of MPSs can lead to an easier path to optimizing the MPS model, which is desirable in our case instead of the single model with a central tensor used in multiple other studies [12] [10].

In both scenarios, the final result after contraction is a vector of length C , where the squared entries of C are proportional to the probability for the input to belong to each given class, i.e. $p(c = i|x) = \frac{1}{Z} \cdot y_i^2$, with $Z = \sum_c y_c^2$ being a normalization constant and y being the output of the MPSs.

In contrast to the typical classification settings, our model's output does not conform to the equation $\sum_{i=1}^C Y_i = 1$, where Y_i is the probability of the class i . This is because our model does not directly compute $p(c = i|x)$. Instead, our classification is determined (in the case of an ensemble of MPSs) by comparing which of the MPSs results in a higher squared value after the contraction with the input. We avoid the commonly used softmax activation function because we aim to generate new samples, and the usual probabilistic constraint set using a softmax activation function would alter the capabilities of the MPS for generating purposes, described later in Sec. II-B2.

The procedure for the forward pass, in the case of a single MPS, is described in Algorithm 1, where we use Einstein summation notation for the tensor contractions.

Algorithm 1 MPS Classification

```

1: procedure CLASSIFICATION(mps, C, input)
2:    $mps_{nlr} \leftarrow \sum_{n,e} mps_{nlre} input_{ne}$ 
3:    $L \leftarrow mps[0, 0]$ 
4:    $R \leftarrow mps[-1, :, 0]$ 
5:   for  $i$  in range(1, N//2) do
6:      $L \leftarrow \sum_r L_r mps[i]_{rl}$ 
7:      $R \leftarrow \sum_l R_l mps[-i]_{rl}$ 
8:   end for
9:    $y \leftarrow \sum_{r,l} L_r C_{crl} R_l$ 
10:  return  $y^2$ 
11: end procedure

```

We adopt the following initialization scheme for our Matrix Product State (MPS):

$$mps[i, :, :, j] = \frac{I_D}{\sqrt{d}}, \quad \forall j \in \{0, \dots, d-1\}, i \in \{1, \dots, N\}. \quad (24)$$

This ensures that each sequential operation on the preceding matrix, i.e. the multiplication of each matrix with the vectors R and L outlined in Algorithm 1, behaves as an identity matrix.

Although past research [44] has explored non-trivial initialization configurations, we opt for this simpler and more intuitive approach which encourages stability during training. The rank-3 tensors present at each network site assume the form $A_s = \frac{I_d}{\sqrt{d}} + \hat{A}^s$, where only \hat{A} is trainable. Each entry of \hat{A} is initialized from a normal distribution $\hat{A}^s \sim \mathcal{N}(0, \sigma^2)$, where σ requires manual adjustment. The introduction of noise serves to disrupt symmetries and prevent convergence to local

minima during the initial stages. Adding weight decay to the model parameters will only affect the matrices $\{\hat{A}^s\}_s$ and will have no effect on the initial settings except to remove the noise, leading to a more stable system during training while using weight decay.

During training, we minimize the cross entropy loss in our classification settings with the ensemble of MPSs, which is equivalent to minimizing the Kullback–Leibler (KL) divergence between a single label model and the data coming from that class, as described in [45].

With this method, we avoid using the DMRG-based method during the optimization of the MPS in [10]. Our approach carries the drawback that it could result in a non-normalized MPS; however, our method addresses this and effectively samples from such non-normalized distributions.

2) *Generation with MPS*: While previous works have employed Metropolis-Hastings and similar Markov chain Monte Carlo-related methods for sampling from MPS models [11][46][47], we perform an exact sampling approach. An iterative method is used to sample coordinate after coordinate from a 1-dimensional non-normalized PDF. A noise vector ν is used as the input of our generative model, where each component ν_i of the noise vector will correspond to the quantile of our sample \hat{x}_i , i.e.:

$$p(x_i \leq \hat{x}_i | x_1, \dots, x_{i-1}) = \nu_i. \quad (25)$$

This technique eliminates the need for MCMC methods, along with their associated bias issues during the sampling process (for example, autocorrelation and burn-in), and is possible due to the process described in Sec. II-A3. Once the ensemble of MPSs has been trained for classification, its unique structure allows us to generate new samples from it. This is facilitated by the fact that any probability distribution over multiple variables can be expressed as follows, using the chain rule for probabilities:

$$p(x_1, x_2, \dots, x_n) = \prod_{i=1}^n p(x_i | \{x_j\}_{j < i}), \quad (26)$$

and due to the structure of the tensor network and the choice of embedding function, the conditional distributions $p(x_i | \{x_j\}_{j < i})$ can be computed using the reduced density matrix. The sampling procedure is outlined in the following pseudocode for Algorithm 2:

Algorithm 2 MPS Sampling

```

1: procedure SAMPLE(mps,  $\nu$ )
2:    $samples \leftarrow \text{zeros}(N)$ 
3:   for  $i$  in range( $N$ ) do
4:      $V = \text{density\_matrix}(i, \text{mps}, \text{samples})$ 
5:      $\text{pdf}(x) = \phi(x) \cdot V \cdot \phi(x)$ 
6:      $\text{cdf}(x) = \int_{-1}^x \text{pdf}(y) dy$ 
7:      $samples[i] = \text{cdf}^{-1}(\nu[i])$ 
8:   end for
9:   return  $samples$ 
10: end procedure

```

Fig. 5 shows the reduced density matrix produced at step i by Algorithm 2.

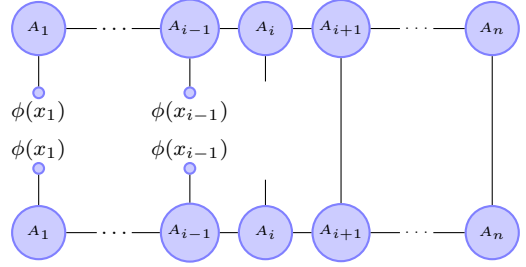


Fig. 5: Visual description of the tensor contractions that produce the matrix $V_{i, \{x_j\}_{j < i}}$, used to calculate the conditional probability $p(x_i | x_1, \dots, x_{i-1}) = \phi(x_i) \cdot V_{i, \{x_j\}_{j < i}} \cdot \phi(x_i)$ during the i -th iteration of our sampling algorithm.

The challenge of the non-normalized MPSs are addressed by normalizing the cumulative distribution functions before sampling from them. An alternative approach could be to calculate the norm of the MPS before each sampling step, and divide each site by the n -th root of the norm, which could be computed using the contractions visualized in Fig. 6, but would require more contraction calculations during training and therefore be less efficient.

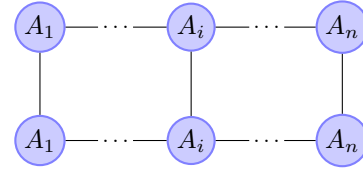


Fig. 6: How to compute the norm of an MPS, using Penrose graphical notation.

The computation of the cumulative probability density and sampling phase must be differentiable in order to apply the methods described in Sec. II-C to facilitate gradient descent during training. If we denote the cumulative distribution function as,

$$f_{V_{i, \{x_j\}_{j < i}}}(x) := \int_{-1}^x \phi(y) \cdot V_{i, \{x_j\}_{j < i}} \cdot \phi(y) dy, \quad (27)$$

we need to compute:

$$\text{sample}(\nu, V_{i, \{x_j\}_{j < i}}) = f_{V_{i, \{x_j\}_{j < i}}}^{-1}(\nu) \quad (28)$$

to obtain a sample given the quantile ν and the reduced density matrix $V_{i, \{x_j\}_{j < i}}$.

Depending on the choice of $\phi(x)$, there may not exist an explicit solution for $f^{-1}(x)$. Hence, the integral is approximated as a finite sum by dividing the input's support into 1000 bins:

$$I(x_k) = \int_{-1}^{x_k} \phi(x) \cdot V \cdot \phi(x) dx = \sum_{i=0}^k \phi(x_i) \cdot V \cdot \phi(x_i) \Delta x, \quad (29)$$

where the bin width is denoted as $\Delta x = \frac{1}{1000}$. We define a set of points as $x_k = k\Delta x$ for $k = 0, 1, 2, \dots, 1000$ in the case

of an embedding function with $\text{Supp}(\Phi) = [0, 1]$. Then, for a given ν within the cumulative density function range, we can approximate the inverse function as follows, opting for linear interpolation between the two closest points:

$$f^{-1}(\nu) \approx x_k + \frac{\nu - I(x_k)}{I(x_{k+1}) - I(x_k)} \cdot \Delta x, \quad (30)$$

where $x_k \leq f^{-1}(\nu) \leq x_{k+1}$. Using this approximation, we can effectively compute the inverse function of the CDF and use it for sampling in Algorithm 2. We generate the vector \mathbf{e} iteratively by sampling points and calculating the conditional reduced density matrix for the next coordinate.

3) *Avoiding vanishing/exploding values in the contractions:* If we want to initialize our MPS as a stable system, because of the sequential nature of the MPSs contraction phase, each of the contractions must be identity operators on the previous tensor; if we initialize each site of the MPS as stated in Eq. 24, the embedding function must then follow the property:

$$\forall x : \sum_k \text{emb}(x)_k = \sqrt{d}. \quad (31)$$

However, this condition, in addition to Eq. 8, would limit the choice for the embedding functions exclude those described in Sec. II-A2, so we decided to opt for an alternative approach.

Given that our model can be represented as a linear model, with the exception of the embedding phase of our data, any subsequent scalar multiplication will not have any influence on the classification and final sampling outcomes. This holds true both during the forward pass of the MPS, as well as in instances involving contraction for the derivation of the density matrix $V_{i, \{x_j\}_{j < i}}$.

To solve the problem of exploding and vanishing values, at each site of the MPS, we divide the vectors of the contraction, i.e. the variables denoted by L and R in Algo. 1, by the value of their largest component after each step. In this way, we will always obtain vectors with a norm contained in the interval $[1, \sqrt{d}]$, avoiding both vanishing and exploding values.

A similar technique is implemented during the computation of the reduced density matrix. Specifically, the matrix is divided by the absolute value of its maximum entry, since the non-normalized PDF defined by Eq. 10 will not be affected by any positive scalar multiplication, allowing us to use the sampling technique in Sec. II-B2 even after rescaling the matrices.

C. MPS for simultaneous classification and generation

As discussed in Sec. II-B2, an MPS trained for classification can be used as a generator to emulate the data that was fed during training. However, this procedure would produce a lot of outliers that does not accurately reproduce the original data [42]. A solution proposed in [42] is to accept generated samples only if the MPS itself outputs a high enough probability that the sample is in the correct class; otherwise, if the output is lower than a pre-determined threshold, the sample is rejected. This removes most outliers in a post-processing step but relies on a manually tuned threshold.

We opt to address this challenge directly from the network architecture to diminish the generation of outliers by using

the MPS as a generator in a GAN-style setting, and letting it compete with a discriminator. There are few regularization techniques for MPS models, for example, weight decay techniques are often used [10], but dropout can not be used easily as in fully connected networks. This GAN-style setting can also be seen as a regularization method of the MPS training. As seen in Sec. III, our GAN-style training produces more realistic samples, without changing the classification accuracy of the model. Here is an overview of our, MPS-GAN, training process:

- 1) Pre-training the MPS: Before the adversarial training, the MPS can be pre-trained using a classification-oriented approach to obtain realistic samples. We empirically observe that this step helps the MPS learn the underlying patterns. Note that it is an intensive training, up to acceptable classification accuracy for the model, since we will use the score of this pre-trained model as a baseline for the adversarial-trained model. This is necessary for the classification accuracy of the final generator to be superior to the pretrained MPS.
- 2) Pre-training the discriminator: The discriminator, which can be a fully connected neural network or a specialized network (such as convolutional neural networks in the case of images), is pre-trained on samples generated by the previously trained MPS and the original dataset.
- 3) Adversarial training: The adversarial training iteratively optimizes both the MPS generator and the discriminator.
 - Generator optimization: Generate samples using the MPS, and then optimize it to minimize the discriminator's ability to distinguish between real and generated samples.
 - Discriminator optimization: The discriminator is optimized using the standard GAN objective, where it maximizes the probability of assigning the correct label to real samples and the incorrect label to generated samples.
- 4) Classification accuracy check: the classification accuracy is checked every epoch to ensure it remains above the initial classification accuracy threshold. If ever it falls below this threshold, the model is retrained in the classical classification setting. This step ensures that the generator maintains its classification capabilities.

An ensemble of discriminators for the different labels are used to reduce the number of outliers among the sample points, while also helping to distinguish between classes. It also prevents samples being wrongly identified as real samples if they are unlabeled and assigned to the false class.

III. RESULTS AND DISCUSSION

The results section will primarily concentrate on the generative performance of our method, as our primary objective is to enhance the network's generative capabilities. During the following experiments, we will search for the best MPS model, according to its classification accuracy,

We demonstrate the generation capabilities of the GAN-style MPS and showcase an analysis of the latent space. The parameters are set in the space $D, d \in \{4, 10, 30\}$, $\sigma = 0.1$

for the initialization, and $lr = 0.01$ as the initial learning rate. Additionally, we incorporate learning rate decay and early stopping procedures.

A. GAN-style training

In this section, the generative performances of the MPS models are analyzed pre- and post-GAN-style training, with comparisons between Fourier and Legendre embedding functions.

An FID-like score is used to compare the generated samples before and after training the MPS in a GAN-style setting. For a training dataset x_1, \dots, x_n and a set of generated samples $x_1^{(g)}, \dots, x_m^{(g)}$, we denote the respective means as $\hat{\mu}$ and $\hat{\mu}^{(g)}$, and the covariance matrices as $\hat{\Sigma}$ and $\hat{\Sigma}^{(g)}$. The FID-like metric is defined as

$$\|\hat{\mu} - \hat{\mu}^{(g)}\|^2 + \text{Tr}(\hat{\Sigma} + \hat{\Sigma}^{(g)} - 2(\hat{\Sigma}\hat{\Sigma}^{(g)})^{1/2}). \quad (32)$$

This metric quantifies the dissimilarity between the real and generated data based on their means and covariance matrices, where a lower value indicates greater similarity between the two datasets.

TABLE I: Comparison of FID-like score (lower is better) on generated samples for Fourier and Legendre embedding functions, pre- and post- GAN-style training

Methods	Datasets		
	2D Spiral	2 Moon	Iris
Legendre, pre-GAN	4.63×10^{-3}	1.20×10^{-2}	6.36×10^{-2}
Fourier, pre-GAN	3.25×10^{-3}	8.79×10^{-4}	1.02×10^{-1}
Legendre, post-GAN	4.57×10^{-3}	5.93×10^{-3}	4.04×10^{-2}
Fourier, post-GAN	1.52×10^{-3}	3.02×10^{-4}	1.96×10^{-2}

The results for both Legendre and Fourier embeddings pre and post-GAN-style training are shown in Table I. The Fourier embedding after the GAN-style training generated the lowest FID-like score across all datasets.

Fig. 7 8 9 also visually show how GAN-style training affects the result of the samples generated by the ensemble of MPSs.

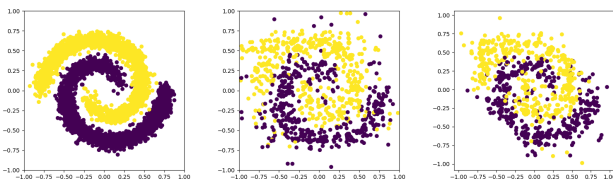


Fig. 7: From left to right: original spiral dataset, samples from the classical trained MPS, samples from the adversarial trained MPS. Both MPSs used Fourier embedding.

The number of outliers generated by the model decreases after the GAN-style training, as shown in Table II which compares the number of outliers before and after the GAN-style training and for different choices for the embedding functions. We evaluate the percentage of outlier samples, where a sample point is considered an outlier if the average

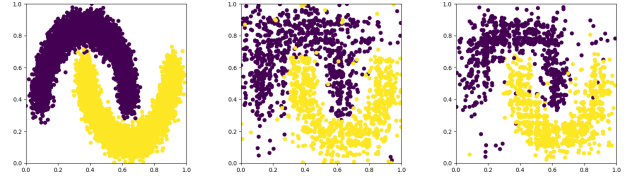


Fig. 8: From left to right: original 2 moon dataset, samples from the classically trained MPS, samples from the adversarial trained MPS.

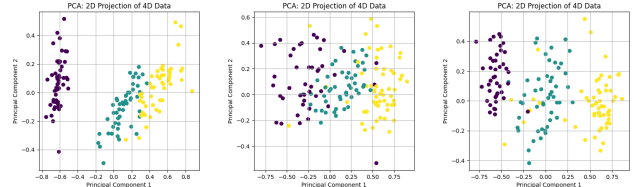


Fig. 9: Plot of the two main principal components of the Iris dataset and sampled data from MPSs with Fourier embedding. From left to right: projection of the original dataset, projection of samples from the classical trained MPS, and projection of samples from the adversarial trained MPS.

of its k-nearest neighbors in the training data is higher than the maximum k-distance of the original dataset.

The values reported in Table II confirm the hypothesis suggested visually by Fig. 7 8 9, where the number of outliers decreases thanks to the GAN-style training. Additionally, the performances of the models that use Fourier embedding functions have lower FID-like scores across the board compared to those resulting from the Legendre embeddings.

B. Latent space analysis

Within our experimental framework, the latent space dimensionality of our generative model, which follows GAN principles, corresponds to the dataset’s dimensionality. For an ideally trained model, every point within this latent space represents a realistic sample. Consequently, conventional latent space analyses, such as clustering of classes within this latent space, become inapplicable.

In scenarios where the PDF is strictly positive and is modeled using the MPS framework, the latent space can be mathematically represented as the hypercube $[0, 1]^n$. Furthermore, there exists a one-to-one mapping (bijection) between this latent space and the physical data space. Consequently, any topological analysis conducted within the latent space yields trivial results due to the direct correspondence between the latent space and the data’s physical space.

However, latent space analysis can be performed thanks to the utilization of the MPS architecture in our experimental setup which is itself an ensemble of models, with each model dedicated to a distinct class. This architecture enables us to perform interpolation and comparison exclusively between intra-class samples. A visual representation of this process is presented in Fig. 10, where two instances of linear interpolation within the latent space are depicted, one for each

TABLE II: Comparison of outlier percentages of generated samples for Fourier and Legendre embedding functions, before and after GAN-style training

Methods	Datasets		
	2D Spiral	2 Moon	Iris
Legendre, pre-GAN	9.03×10^{-2}	1.00×10^{-1}	3.60×10^{-1}
Fourier, pre-GAN	8.90×10^{-2}	1.13×10^{-1}	4.62×10^{-1}
Legendre, post-GAN	7.63×10^{-2}	1.00×10^{-1}	2.20×10^{-1}
Fourier, post-GAN	6.32×10^{-2}	3.40×10^{-2}	2.36×10^{-1}

class, employing different Fourier and Legendre embedding functions.

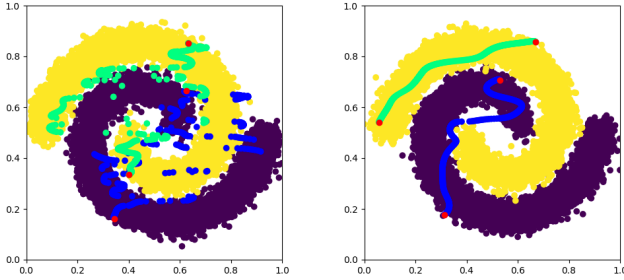


Fig. 10: In the background the original dataset, and in green and blue the trajectories of samples for Fourier (on the left) and Legendre (on the right) embedding functions, corresponding to the yellow and violet class respectively. The trajectories are obtained by linearly interpolating 2 points of the latent space of the MPS, highlighted in red.

The trajectories associated with the Legendre embedded data form a much more regular shape, while the Fourier ones seem to be a lot more chaotic. However, in both cases, the vast majority of the samples composing the trajectories are contained within the correct label, with limited exceptions. One such exception occurs in low probability zones, where the intersection of the trajectories into the false class is inevitable. This results from the non-zero probability of sampling the false class due to the MPS structure.

C. Robustness to perturbations

We assumed that our model has an input space on $[0, 1]^N$, and that the embedding function used in this work transforms the data onto an n -dimensional manifold in a $d \cdot n$ dimensional space. In this section, we consider how adding noise to this manifold can change the performance of the MPS model, depending on the choice of the embedding function. After obtaining a trained MPS, the classification accuracy of the model is observed for increasing values of σ , which determines the amount of noise ϵ that is added to the inputs of the MPS after having embedded the data using $\Phi(x)$, with $\epsilon \sim \mathcal{N}(0, \sigma^2)$.

Fig. 11 shows the accuracy performance of two models, one with Fourier and the other with Legendre embedding function, as noise is added to the embedded inputs.

The model with the Legendre embedding, which starts with a higher validation accuracy, drops significantly faster than

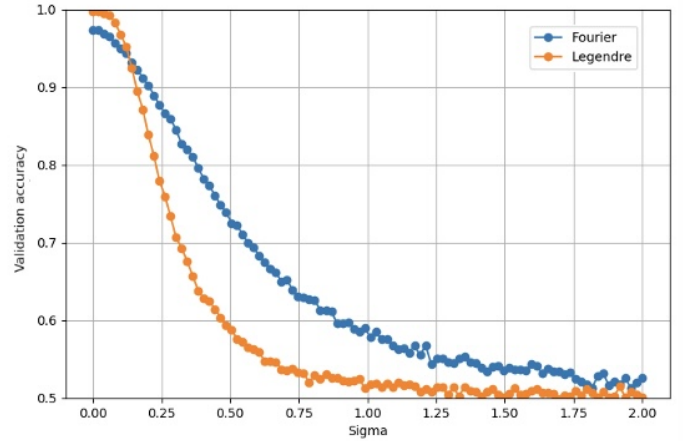


Fig. 11: Accuracy on the validation set as a function of σ , that represents the standard deviation of the normal distribution with mean 0 where we sampled the noise added to the embedded inputs. Comparison between Fourier and Legendre embedding.

the one using Fourier embedding, which indicates a higher resistance to perturbations.

IV. CONCLUSION AND FUTURE WORK

In this study, we explore the MPS and its applications in the field of machine learning. We demonstrate the fundamental structure of MPS and its utility in machine learning for tasks related to classification and generative modeling. We expound upon the various canonical forms of MPS and justify a more accessible training approach for its applications in machine learning, specifically avoiding the necessity for the sweeping algorithm.

To facilitate the discussion, we identified and examined the essential criteria for an embedding function that enables accurate sampling from a non-normalized model trained for classification. We demonstrate the computation of the reduced density matrix and establish its positive semi-definiteness. Furthermore, we introduce and contrast the widely adopted Fourier embedding with our novel proposition of using Legendre polynomials. Our empirical findings indicate that the former yields superior generative results.

Building upon principles from GANs, we leverage dual roles of the MPS, allowing it to serve both as a generator and a classifier simultaneously. This enhances training and generative performance without compromising the model's classification accuracy. Notably, this approach results in a reduction of the number of outliers generated during the sampling process, yielding samples with more favorable FID-like scores when compared to classical training techniques for MPSs.

Within the framework of this procedure, we introduce a latent space representation for the MPS model when using it as a generator and subject it to analysis. We investigate the impact of introducing perturbations after data embedding on the classification accuracy for both Fourier and Legendre

embeddings, where the former demonstrated greater resilience in the presence of increasing noise.

In further research, alternative embedding functions can be explored. For instance, the use of the Welsh basis, a non-continuous set of orthonormal functions, warrants exploration. Additionally, investigating non-orthogonal bases is promising, leveraging the research developed in this work on the role of the embedding function in calculating the reduced density matrix. Furthermore, it is interesting to investigate how perturbations may impact the classification accuracy, particularly when various embedding functions are employed. Furthermore, the MPS holds promise for integration with other neural network paradigms, potentially as a latent space representation within a variational autoencoder or a normalizing flow in manifold learning frameworks [48], where the density can be directly estimated mitigating the need of approximate inference.

REFERENCES

- [1] R. K. Ramakrishnan, A. B. Ravichandran, A. Mishra, *et al.*, “Integrated photonic platforms for quantum technology: A review,” *ISSS Journal of Micro and Smart Systems*, vol. 12, no. 2, pp. 83–104, 2023, ISSN: 2509-7997. DOI: 10.1007/s41683-023-00115-1. [Online]. Available: <https://doi.org/10.1007/s41683-023-00115-1>.
- [2] T. Suzuki, T. Hasebe, and T. Miyazaki, “Quantum support vector machines for classification and regression on a trapped-ion quantum computer,” *Quantum Machine Intelligence*, vol. 6, no. 1, p. 31, 2024, ISSN: 2524-4914. DOI: 10.1007/s42484-024-00165-0. [Online]. Available: <https://doi.org/10.1007/s42484-024-00165-0>.
- [3] M. Hdaib, S. Rajasegarar, and L. Pan, “Quantum deep learning-based anomaly detection for enhanced network security,” *Quantum Machine Intelligence*, vol. 6, no. 1, p. 26, 2024, ISSN: 2524-4914. DOI: 10.1007/s42484-024-00163-2. [Online]. Available: <https://doi.org/10.1007/s42484-024-00163-2>.
- [4] J. Biamonte and V. Bergholm, “Tensor networks in a nutshell,” *arXiv preprint arXiv:1708.00006*, 2017.
- [5] A. M. Dalzell and F. G. Brandão, “Locally accurate mps approximations for ground states of one-dimensional gapped local hamiltonians,” *Quantum*, vol. 3, p. 187, 2019.
- [6] R. Orús, “Tensor networks for complex quantum systems,” *Nature Reviews Physics*, vol. 1, no. 9, pp. 538–550, 2019.
- [7] J. A. Bengua *et al.*, “Matrix product state for higher-order tensor compression and classification,” *IEEE Transactions on Signal Processing*, vol. 65, no. 15, pp. 4019–4030, 2017.
- [8] A. Pozas-Kerstjens, S. Hernández-Santana, J. R. P. Monturiol, *et al.*, *Privacy-preserving machine learning with tensor networks*, 2023. arXiv: 2202.12319 [cs.CR].
- [9] W. E. J. Han, and A. Jentzen, “Algorithms for solving high dimensional pdes: From nonlinear monte carlo to machine learning,” *Nonlinearity*, vol. 35, no. 1, pp. 278–310, Dec. 2021, ISSN: 1361-6544. DOI: 10.1088/1361-6544/ac337f. [Online]. Available: <http://dx.doi.org/10.1088/1361-6544/ac337f>.
- [10] E. Miles and Schwab, “Supervised learning with quantum-inspired tensor networks,” p. 4799, 2016.
- [11] Z.-Y. Han *et al.*, “Unsupervised generative modeling using matrix product states,” *Physical Review X*, vol. 8, no. 3, p. 031012, 2018.
- [12] S. Cheng, L. Wang, and P. Zhang, “Supervised learning with projected entangled pair states,” *Physical Review B*, vol. 103, no. 12, p. 125117, 2021.
- [13] T. Vieijra, L. Vanderstraeten, and F. Verstraete, “Generative modeling with projected entangled-pair states,” *arXiv preprint arXiv:2202.08177*, 2022.
- [14] I. Glasser *et al.*, “Expressive power of tensor-network factorizations for probabilistic modeling,” 2019.

- [15] G. Vidal, “Entanglement renormalization,” *Physical review letters*, vol. 99, no. 22, p. 220405, 2007.
- [16] S. Cheng *et al.*, “Tree tensor networks for generative modeling,” *Physical Review B*, vol. 99, no. 15, p. 155131, 2019.
- [17] M. P. Zaletel and F. Pollmann, “Isometric tensor network states in two dimensions,” *Phys. Rev. Lett.*, vol. 124, p. 037201, 3 Jan. 2020. DOI: 10.1103/PhysRevLett.124.037201. [Online]. Available: <https://link.aps.org/doi/10.1103/PhysRevLett.124.037201>.
- [18] R. Orús, “A practical introduction to tensor networks: Matrix product states and projected entangled pair states,” *Ann. Phys.*, vol. 349, p. 117, 2014.
- [19] D. Perez-Garcia *et al.*, “Matrix product state representations,” *arXiv preprint quant-ph/0608197*, 2006.
- [20] F. Verstraete and J. I. Cirac, “Matrix product states represent ground states faithfully,” *Physical review b*, vol. 73, no. 9, p. 094423, 2006.
- [21] M. B. Hastings, “An area law for one-dimensional quantum systems,” *Journal of statistical mechanics: theory and experiment*, P08024, 2007.
- [22] J. C. Bridgeman and C. T. Chubb, “Hand-waving and interpretive dance: An introductory course on tensor networks,” *Journal of physics A: Mathematical and theoretical*, vol. 50, no. 22, p. 223001, 2017.
- [23] B. Bruognolo *et al.*, “Matrix product state techniques for two-dimensional systems at finite temperature,” *arXiv preprint arXiv:1705.05578*, 2017.
- [24] “Mnist handwritten digit database.” (), [Online]. Available: <http://yann.lecun.com/exdb/mnist/>.
- [25] H. Xiao, K. Rasul, and R. Vollgraf, “Fashion-mnist: A novel image dataset for benchmarking machine learning algorithms,” *arXiv preprint arXiv:1708.07747*, 2017.
- [26] S. Efthymiou, J. Hidary, and S. Leichenauer, “Tensor network for machine learning,” *arXiv preprint arXiv:1906.06329*, 2019.
- [27] H.-J. Liao, J.-G. Liu, L. Wang, and T. Xiang, “Differentiable programming tensor networks,” *Phys. Rev. X*, vol. 9, p. 031041, 3 Sep. 2019. DOI: 10.1103/PhysRevX.9.031041. [Online]. Available: <https://link.aps.org/doi/10.1103/PhysRevX.9.031041>.
- [28] A. Francuz, N. Schuch, and B. Vanhecke, *Stable and efficient differentiation of tensor network algorithms*, 2023. arXiv: 2311.11894 [quant-ph].
- [29] C. M. Bishop, *Pattern Recognition and Machine Learning (Information Science and Statistics)*. Berlin, Heidelberg: Springer-Verlag, 2006, ISBN: 0387310738.
- [30] R. Penrose, “Applications of negative dimensional tensors,” pp. 221–244, 1971.
- [31] U. Schollwöck, “The density-matrix renormalization group in the age of matrix product states,” *Annals of Physics*, vol. 326, no. 1, pp. 96–192, 2011.
- [32] S. R. White, “Density matrix formulation for quantum renormalization groups,” *Physical review letters*, vol. 69, no. 19, p. 2863, 1992.
- [33] S. R. White, “Density-matrix algorithms for quantum renormalization groups,” *Physical review b*, vol. 48, no. 14, p. 10345, 1993.
- [34] A. Pozas-Kerstjens, “Privacy-preserving machine learning with tensor networks,” *Bulletin of the American Physical Society*, 2023.
- [35] J. Haegeman, C. Lubich, I. Oseledets, B. Vandereycken, and F. Verstraete, “Unifying time evolution and optimization with matrix product states,” *Physical Review B*, vol. 94, no. 16, p. 165116, 2016.
- [36] “Matrix product states: Canonical forms.” (), [Online]. Available: <https://muellergroup.lasp.cornell.edu/bt2020chap4.pdf>.
- [37] G. K. Chan *et al.*, “Matrix product operators, matrix product states, and ab initio density matrix renormalization group algorithms,” *The Journal of chemical physics*, vol. 145, no. 1, 2016.
- [38] I. V. Oseledets, “Tensor-train decomposition,” *SIAM Journal on Scientific Computing*, vol. 33, no. 5, pp. 2295–2317, 2011.
- [39] J. Håstad, “Tensor rank is np-complete,” 1989.
- [40] V. De Silva and L.-H. Lim, “Tensor rank and the ill-posedness of the best low-rank approximation problem,” *SIAM Journal on Matrix Analysis and Applications*, vol. 30, no. 3, pp. 1084–1127, 2008.
- [41] A. Paszke *et al.*, “Automatic differentiation in pytorch,” 2017.
- [42] B. Žunkovič, “Positive unlabeled learning with tensor networks,” *Neurocomputing*, p. 126556, 2023.
- [43] A. J. Ferris and G. Vidal, “Perfect sampling with unitary tensor networks,” *Physical Review B*, vol. 85, no. 16, p. 165146, 2012.
- [44] O. Hrinchuk, V. Khrulkov, L. Mirvakhabova, E. Orlova, and I. Oseledets, “Tensorized embedding layers for efficient model compression,” *arXiv preprint arXiv:1901.10787*, 2019.
- [45] J. Liu *et al.*, “Tensor networks for unsupervised machine learning,” *Physical Review E*, vol. 107, no. 1, p. L012103, 2023.
- [46] R. Bonnevie and M. N. Schmidt, “Matrix product states for inference in discrete probabilistic models,” *The Journal of Machine Learning Research*, vol. 22, no. 1, pp. 8396–8443, 2021.
- [47] A. J. Ferris, “Unbiased monte carlo for the age of tensor networks,” *arXiv preprint arXiv:1507.00767*, 2015.
- [48] K. Flouris and E. Konukoglu, “Canonical normalizing flows for manifold learning,” in *Advances in Neural Information Processing Systems*, A. Oh, T. Naumann, A. Globerson, K. Saenko, M. Hardt, and S. Levine, Eds., vol. 36, Curran Associates, Inc., 2023, pp. 27294–27314. [Online]. Available: https://proceedings.neurips.cc/paper_files/paper/2023/file/572a6f16ec44f794fb3e0f8a310acbc6-Paper-Conference.pdf.